Accepted Manuscript

Potholing of the hydrophobic heme oxygenase-1 western region for the search of potent and selective imidazole-based inhibitors

Loredana Salerno, Emanuele Amata, Giuseppe Romeo, Agostino Marrazzo, Orazio Prezzavento, Giuseppe Floresta, Valeria Sorrenti, Ignazio Barbagallo, Antonio Rescifina, Valeria Pittalà

PII: S0223-5234(18)30129-6

DOI: 10.1016/j.ejmech.2018.02.007

Reference: EJMECH 10184

To appear in: *European Journal of Medicinal Chemistry*

Received Date: 8 December 2017

Revised Date: 29 January 2018

Accepted Date: 3 February 2018

Please cite this article as: L. Salerno, E. Amata, G. Romeo, A. Marrazzo, O. Prezzavento, G. Floresta, V. Sorrenti, I. Barbagallo, A. Rescifina, V. Pittalà, Potholing of the hydrophobic heme oxygenase-1 western region for the search of potent and selective imidazole-based inhibitors, *European Journal of Medicinal Chemistry* (2018), doi: 10.1016/j.ejmech.2018.02.007.

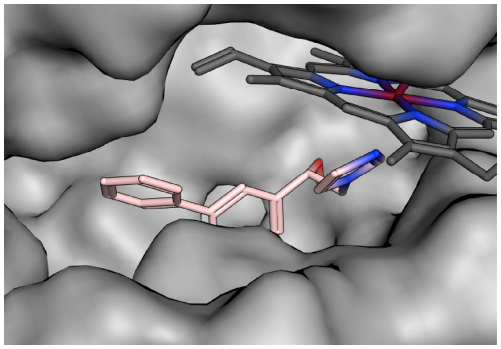

Compound	IC_{50} (μM) HO-1	HO-2	HO-2/HO-1
1b	0.90 ±0.08	>100	>111
1j	0.95 ±0.02	>100	>105

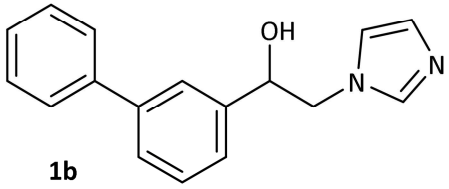

1b

Potholing of the hydrophobic heme oxygenase-1 western region for the search of potent and selective imidazole-based inhibitors

Loredana Salerno [a], Emanuele Amata [a], Giuseppe Romeo [a], Agostino Marrazzo [a], Orazio Prezzavento [a], Giuseppe Floresta [a,b], Valeria Sorrenti [a], Ignazio Barbagallo [a], Antonio Rescifina [a,*], Valeria Pittalà [a,**]

[a] Department of Drug Sciences, University of Catania, V.le A. Doria 6, 95125 Catania, Italy

[b] Department of Chemical Sciences, University of Catania, V.le A. Doria, 95125 Catania, Italy

Corresponding authors:

Antonio Rescifina arescifina@unict.it

Valeria Pittalà vpittala@unict.it

Graphical abstract

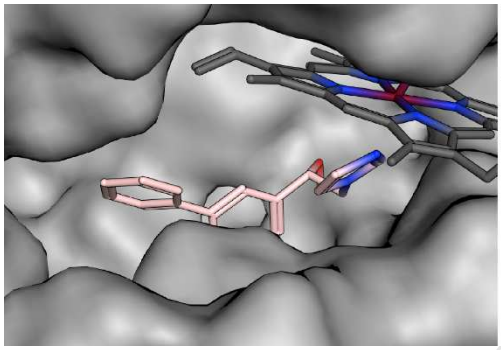

Compound	IC_{50} (μM) HO-1	HO-2	HO-2/HO-1
1b	0.90 ±0.08	>100	>111
1j	0.95 ±0.02	>100	>105

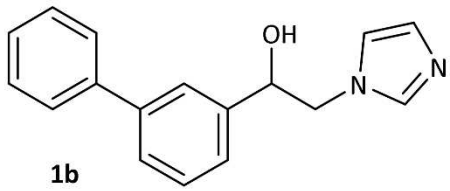

1b

Highlights

- New imidazole-based HO-1 inhibitors have been synthesized
- The molecules act as potent HO-1 inhibitors as confirmed by the biological assay
- Two molecules show a selectivity >100 toward HO-1 respect to HO-2
- *In silico* studies suggest the binding poses and the ADME-Toxicity profile

Keywords: Heme oxygenase-1 western region, HO-1 imidazole inhibitors, Docking studies, *In silico* profiling, ADME-Toxicity.

Abstract

Here we report the design, synthesis, and molecular modeling of new potent and selective imidazole-based HO-1 inhibitors in which the imidazole nucleus and the hydrophobic groups are linked by a phenylethanolic spacer. Most of the tested compounds showed a good inhibitor activity with IC_{50} values in the low micromolar range, with two of them (**1b** and **1j**) exhibiting also high selectivity toward HO-2. These results were obtained by the idea of potholing the entire volume of the principal hydrophobic western region with an appropriate ligand volume. Molecular modeling studies showed that these molecules bind to the HO-1 in the consolidated fashion where the imidazolyl moiety coordinates the heme iron while the aromatic groups are stabilized by hydrophobic interaction in the western region of the binding pocket. Finally, the synthesized compounds were analyzed for *in silico* ADME-Tox properties to establish oral drug-like behavior and showed satisfactory results.

1. Introduction

Heme levels are endogenously regulated by the heme oxygenase (HO) enzyme family. Heme catabolism reaction mediated by HO produces an equimolar amount of Fe^{2+}, carbon monoxide (CO), and biliverdin (BV) which is readily converted into bilirubin (BR) by biliverdin reductase. Two major isoforms of HO exist, HO-1 and HO-2. HO-1 (32 kDa), is physiologically expressed at low levels in the whole human body and more abundantly in spleen and liver. HO-1 is a strongly inducible isoform and is also referred as heat shock protein 32 (Hsp32). HO-2 (37 kDa) is a non-inducible constitutive form, mainly found in brain and testis, whose physiological roles have not yet been fully elucidated [1, 2].

A wide array of stimuli including oxidative, heat shock, heavy metals, UV radiations, and heme itself are able to upregulate HO-1 which in turn, removing the pro-oxidant heme and forming CO and BV products, exerts a significant cytoprotective role [3-5]. The HO-1 induction is widely acknowledged as an adaptive cellular response able to counteract oxidative stress. Moreover, it is also suggested that both HO-1 and fatty acid binding proteins may have complementary or synergistic antioxidant effects [6, 7]. HO-1 establishes a protective effect on cells and tissues against injuries related to pathological conditions as diabetes, obesity, cardiovascular and pulmonary disorders [3, 8-13]. In this regard, HO-1 inducers may play a role in the management of the abovementioned diseases [10].

At the same time, the HO-1 inhibition is reported to be beneficial for some pathological conditions including neonatal jaundice and some type of cancers. Jaundice in newborns is characterized by an augmented production of BR. The HO-1 inhibition giving a reduction of heme catabolism and BR formation may be considered a valuable route for neonatal jaundice management [14, 15].

High levels of HO-1 have been frequently reported in different human cancers. Patients showing HO-1 overexpression are reported to have statistically lower survival rate and poor outcomes [16]. Notwithstanding, the involvement of HO-1 in cancer is not fully clarified. The HO-1 protumoral action seems to be closely linked to its cytoprotective, antiapoptotic, and angiogenic actions and

with the modulation of inflammatory and immune responses [16]. Although some papers report a lower expression of HO-1 in cancerous cells, a larger amount of data clearly show that HO-1 levels are notably increased in different cancers including multiple myeloma [17], neuroblastoma (NB), chronic and acute myeloid leukemia [18, 19], breast, prostate, and pancreatic [20]. Moreover, in most cases where cytotoxicity is connected to reactive oxygen species (ROS), HO-1 overexpression has been linked with the onset of resistance towards chemo-, radio-, and photodynamic- cancer therapy [21, 22]. In this perspective, HO-1 inhibitors can be therapeutically useful in cancer treatment and/or be used as potential enhancers under regimens of chemotherapy, radiotherapy, or photodynamic therapy. In this contest, the identification of inhibitors endowed with high affinity and selectivity for HO-1, respect to the constitutive isoform HO-2, may help in better understand the biological roles of this protein and its implication in several human diseases.

The first reported class of competitive HO-1 inhibitors is represented by the heme analogs metalloporphyrins (MPs). These compounds, sharing strong structural homologies with heme, are able to compete with heme itself and to bind other heme-containing enzymes [*e.g.* nitric oxide synthase (NOS), soluble guanylyl cyclase (sGC), and cytochromes (CYPs) P450] [23, 24]. Accordingly, the use of MPs to solve the physio-pathological roles of HO-1 may be questionable and this major limitation, among others, impaired further development of this chemical class.

Other than MPs, only one other class of HO-1 inhibitors deriving from QC-1 (Azalanstat) has been reported [25]. Later on, structure-activity relationship (SAR) studies around Azalanstat and the X-ray crystal studies of QC-15, QC-80, QC-82, QC-86, and QC-308 in complex with HO-1 (Table 1) helped to clarify the essential chemical features required for binding, the binding mode itself, and solved the issue of off-target activity at other heme-containing enzymes [26-31].

These inhibitors are generally identified by a non-competitive binding mode by preventing Fe^{2+} oxidation and interfering with O_2 binding when heme is located within the HO-1 binding pocket. Non-competitive HO-1 inhibitors consist of a hydrophobic moiety, a connecting chain of variable length, and an azole-based structure [32]. The latter is most frequently represented by an imidazole

ring able to coordinate the Fe^{2+} atom of heme when heme itself is bound to the HO-1 heme binding pocket.

Table 1
Chemical structures of selected HO-1 inhibitors, binding regions, and selectivity index (SI).

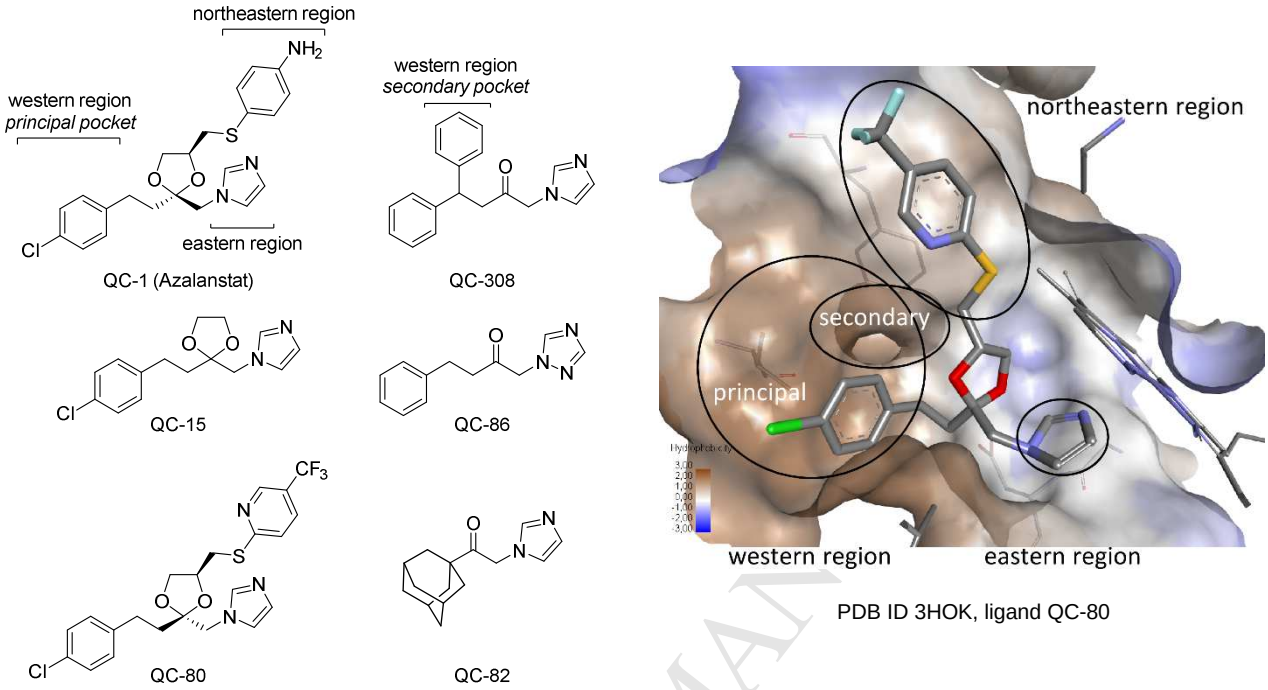

Compound	HO-1 IC_{50} (μM)	HO-2 IC_{50} (μM)	SI (HO-2/HO-1)	PDB ID
QC-1 (Azalanstat)	5.3	24.4	4.4	—
QC-15	2.8	>100	>35.7	2DY5
QC-80	2.1	16	7.6	3HOK
QC-82	3.0	>100	>33.3	3CZY
QC-86	2.5	18	7.2	3K4F
QC-308	0.27	0.46	1.7	3TGM

Recently, our research group has built a ligand database (HemeOxDB, http://www.researchdsf.unict.it/hemeoxdb) that incorporates the whole set of published HO-1 and HO-2 inhibitors, resulting in more than 400 compounds [33]. Among these set, only 32 compounds (7.4%) showed an HO-1 IC_{50} <1 μM and, in this subset, only 4 compounds possessed a HO-2/HO-1 ratio >100. On these grounds and motivated by our ongoing interest in developing potent and selective HO-1 inhibitors [18, 34, 35], here we report the design, synthesis, and molecular modeling of new HO-1 inhibitors in which the imidazole nucleus and the hydrophobic groups are connected by a phenylethanolic chain (Table 2). For all the synthesized compounds we describe the inhibitory activity towards HO-1. For the most interesting compounds (HO-1 IC_{50} values <1 μM) the HO-2 inhibitory activity has also been determined. Finally, an ADME toxicity *in silico* prediction was

carried out for the most promising compounds.

2. Results and Discussion

2.1. Design

According to previously described SARs and crystallographic data [31-33], among azole-based HO-1 inhibitors, the azole moiety, located in the eastern region, serves as an anchor coordinating with the Fe^{2+} atom through nitrogen 3 completing the heme hexacoordination. In addition, the enzyme presents two hydrophobic pockets, one in the proximity region (northeastern) of the heme-binding pocket, and the other in the distal region (western); this last is substantially constituted by a principal large cavity and, lateral to this, a small secondary ones (Table 1) [31]. These pockets have an important role in determining the inhibitor potency by stabilizing the ligand-enzyme binding. Due to the flexibility of these pockets, hydrophobic groups of different size, such as aryl, biphenyl, or adamantly moieties, allocated in the western and/or in the northeastern regions of the ligand, can be accommodated [31, 32]. Moreover, it was ascertained that modifications in the northeastern region result in a moderate gain in HO-2 inhibitory activity and therefore these are not an efficient avenue in the development of highly selective HO-1 inhibitors [36-38]. The occupation of the western secondary small hydrophobic pocket (*double-clamp* ligands, *e.g.* QC-308), although brings to an increase in the HO-1 inhibitory activity, not fulfill the isoform selectivity [30]. Finally, from a careful review of the literature and from the HemeOxDB inspection, it emerged that compounds bearing an alcoholic function in the connecting alkyl chain, most of them characterized by a four methylene chain units, result more active and selective for HO-1 respect to the corresponding ketone analogues [29, 39, 40].

With this in mind, we decided to focus our attention on the potholing of the principal hydrophobic heme oxygenase-1 western region for the search of new potent and selective imidazole-based inhibitors possessing an unadorned imidazole, linked through a phenylethanolic connecting chain to hydrophobic moieties of variable size, preferentially bearing a halogen residue (compounds **1a**–**k**,

Table 2).

These compounds were designed on the basis of the following considerations: *i)* the analyses of the pocket cavity volumes near the heme-prosthetic group in the crystal structures of the HO-1 (PDB ID 1N45) and HO-2 (PDB ID 2QPP) umbound forms revealed a mean difference of about 34 $Å^3$ in favor of the HO-2 (Table S1); *ii)* the analogue analyses conducted on five-known corresponding HO-1/ligand co-crystallized forms (PDB ID 2DY5, 3CZY, 3K4F, 3HOK, and 3TGM) showed that the volume of the binding pocket is quite flexible and adaptable to that of the ligands and increase with the size of the enclosed molecule (Table S1); *iii)* the four most potent and selective HO-1 inhibitors with IC_{50} <1 μM and HO-2/HO-1 >100 possess a mean Van der Waals volume of 274.34 $Å^3$ with an interval of 239.00–302.87 $Å^3$ (Table S1); *iv)* inspection of the HemeOxDB for the most potent and selective HO-2 inhibitors (IC_{50} <1 μM and HO-1/HO-2 >40) gives out four compounds with a mean Van der Waals volume of 284.10 $Å^3$ with an interval of 274.37–306.75 $Å^3$ (Table S1). These observations, taken altogether, highlighted that the volume of the ligands, simplistically, could be an important factor influencing the selectivity; thus, the larger the cavity of the initial unbound isoform, the greater the volume of the ligand to achieve the best binding potency and selectivity. To prove this assumption, the volumes of designed compounds **1a**–**k** encompass the interval 219.12–329.87 $Å^3$, calculated for the most stable conformer (Table S2).

Table 2
General structure of compounds **1a**–**k**.

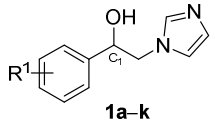

1a–**k**

Compound	R^1
1a	3-Br
1b	3-Ph
1c	4-I
1d	4-Ph
1e	4-(4′-ClC_6H_4)
1f	4-PhO
1g	4-$PhCH_2$
1h	4-$PhCH_2O$
1i	4-(4-ClC_6H_4)CH_2O
1j	4-(4-BrC_6H_4)CH_2O
1k	4-(4-IC_6H_4)CH_2O

2.2. Synthesis

Compounds **1a**–**k** have been synthesized according to the general pathway illustrated in Scheme 1. Intermediates **3a**–**i** were synthesized by nucleophilic displacement of the commercially available 1-substituted bromomethyl ketones **2a**–**i** using an excess of imidazole. The 1-substituted bromomethyl ketones **2j**,**k** were obtained by bromination [41], in the glacial acetic acid, of the corresponding commercially available ketones and used as it to synthesize compounds **3j**,**k** as reported above. The imidazole ketones **3a**–**k**, were then reduced with $NaBH_4$ affording the final compounds **1a**–**k** in high yield.

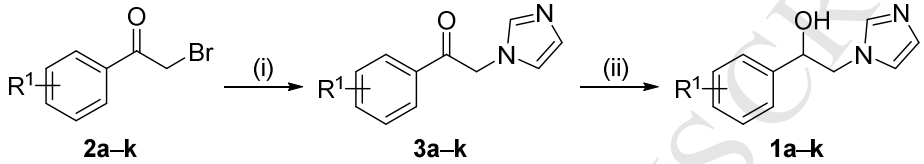

Scheme 1. Reagents and conditions: (i) imidazole, K_2CO_3, dry DMF, room temperature, 2 h, then water; (ii) $NaBH_4$, CH_3OH, 2 h, reflux, then HCl 1N, 0.5 h, reflux.

2.3. HO inhibition and structure-activity relationships (SARs)

For inhibitory activity assay, HO-1 and HO-2 have been extracted from rat spleen and rat brain microsomal fractions, respectively. Enzyme activity inhibition is expressed as IC_{50} (μM) and results are outlined in Table 3, utilizing Azalanstat as reference compound. All the novel synthesized derivatives exhibited good inhibitory potency towards HO-1. Only compounds which showed HO-1 IC_{50} values <1 μM, were tested on HO-2. Above all, compounds **1a**, **1b**, **1f**, **1h**, and **1j** stand out for their potency on HO-1 (IC_{50} <1 μM), and a couple of them showed a remarkable selectivity towards HO-2.

Table 3
Inhibitory potency and selectivity index (SI) of compounds **1a–k** towards HO-1 and HO-2.

Compound	IC_{50} (μM)[a]		SI (HO-2/HO-1)
	HO-1	HO-2	
1a	0.40 ±0.01	32.00 ±2.2	80
1b	0.90 ±0.08	>100	>111
1c	14.80 ±0.8	ND[b]	—
1d	11.70 ±0.3	ND[b]	—
1e	26.90 ±0.8	ND[b]	—
1f	0.90 ±0.1	10.50 ±0.2	11.6
1g	26.90 ±1.1	ND[b]	—
1h	0.50 ±0.01	11.70 ±0.9	23.4
1i	13.10 ±0.9	ND[b]	—

1j	0.95 ±0.02	>100	>105
1k	24.50 ±1.0	ND[b]	—
Azalanstat	5.30 ±0.4	24.40 ±0.8	4.6

[a] Data are shown as IC_{50} values in μM ± standard deviation (SD). Values are the mean of triplicate experiments.
[b] ND = not determined. The HO-2 activity was determined only for those compounds with an HO-1 IC_{50}<1 μM.

Compound **1a**, possessing a bromine residue at the 3-position of the phenyl ring, demonstrated to be more active (IC_{50} = 0.40 μM) than compound **1c** bearing an iodine at the 4-position (HO-1 IC_{50} = 14.80 μM). The bromo-derivate **1a** gave good results also in terms of HO-2/HO-1 selectivity, although this ratio was not satisfactory when compared to HO-1 inhibitors reported so far [38-40]. When the second phenyl ring is directly linked to the first one, as in the plain or 4-chlorosubstituted biphenyl derivatives **1d** and **1e**, we observed a decrease of HO-1 activity (HO-1 IC_{50} = 11.70 μM and IC_{50} = 26.90 μM, respectively), compared with **1a**. Conversely, when the second phenyl ring is linked at the 3-position, as in compound **1b**, the inhibitory activity reach an IC_{50} value of 0.95 μM coupled with an optimal selectivity towards the HO-2 isoform (IC_{50} > 100 μM).

When the second phenyl ring is separated by a methylene bridge, as for compound **1g**, a similar trend with respect to compounds **1d** and **1e** was observed, being **1g** HO-1 IC_{50} = 26.90 μM. Conversely, compound **1f**, possessing a diphenyl ether residue, showed a 30-fold increase in inhibitory potency (HO-1 IC_{50} = 0.90 μM). Unfortunately, this compound also significantly inhibited HO-2. The elongation of the spacer between the two phenyl rings afforded compounds **1h**,**k**. The potency of these four compounds was strongly influenced by the substituent of the second phenyl ring, being the unsubstituted **1h** and the 4-iodophenyl substituted **1k**, respectively, the best and the worse HO-1 inhibitors in this subset. In term of selectivity, compound **1j** demonstrated good potency towards HO-1 (IC_{50} = 0.95 μM), and remarkable selectivity against HO-2 (IC_{50} >100 μM).

Interestingly, the most potent and selective compound **1b** has a calculated Van der Waals volume of 275.12 $Å^3$ that is the nearest to the mean value of 274.34 $Å^3$ calculated on the best four potent and selective compounds (Table S2), according to the postulated assumption on the relation between cavity volumes and potency/selectivity.

2.4. Docking studies

After the publication of various imidazole derivatives in complex with HO-1 (ID PDB, Table 1), different docking studies were successfully performed for understanding the ligand-protein interactions [34, 42]. In order to figure out the key interactions of our new compounds, we investigated the binding modes of **1a**–**k** using the crystal structure of HO-1 complexed with QC-80 (ID PDB 3HOK) in order to explore the largest binding pocket and, at the same time to exclude the involvement of the northeastern cavity. Docking was performed using AutoDock [43] and the setup was done with the YASARA molecular modeling program [44].

To validate the docking model, and to ascertain that the choice of the largest pocket does not excessively invalidate the results with the less bulky ligands, we docked the Azalanstat and the five co-crystallized ligands (QC-15, QC-80, QC-82, QC-86, and QC-308) in the binding pocket of the 3HOK structure. The results reported in Table 4 show that the calculated binding potencies are in good agreement with the experimental ones. Moreover, the docked pose of the original ligand QC-80 shows high analogy to the corresponding crystallographic structure with an RMSD value of 0.75 Å.

Table 4
Docking results for Azalanstat and co-crystallized ligands.

Compound	ΔG_B (kcal/mol)	K_i calcd (μM)	IC_{50} exp (μM) HO-1
Azalanstat	–7.45	3.4	5.3
QC-15	–7.59	2.7	4.0
QC-80	–7.04	6.8	2.1
QC-82	–7.55	2.9	3.0
QC-86	–6.63	13.7	2.5
QC-308	–8.11	1.1	0.27

Since our compounds present a stereocenter (at the C_1 ethanolic position, Table 2), we performed a preliminary docking study on both stereoisomers of the most potent compound **1a** to verify the eventual existence of an eudysmic ratio; the obtained results highlighted only a very small difference in the calculated binding energy in favor of the (*S*)-enantiomer (0.02 kcal/mol), because the hydroxylic moiety occupying the hydrophobic region not establish any hydrogen bond (Fig. S1).

Moreover, the superimposition of the binding pose of QC-80 ligand, possessing the 1,3-dioxolane ring, to the binding poses of the two enantiomers of compound **1a**, shows that the oxygen atoms of the two enantiomers occupy the same three-dimensional space as those of the dioxolane moiety without any possibility to establish an opportune non-bonding interaction (Fig. S2), so justifying the possible absence of an eudysmic ratio. Thus, once validated the model, we focused the attention only on the (*S*)-enantiomer of compounds **1a**–**k** docking them into the active site (encompassing all the hydrophobic cavities) of HO-1. The results are collected in Table 5 and the docking poses are shown in Fig. S3.

All docked compounds correctly present the ferrous iron of heme coordinated by the nitrogen atom of the imidazole ring (eastern pocket). By means of this coordination binding, Fe^{2+} is protected from oxidation by disruption of an ordered solvent structure involving the critical Asp140 hydrogen-bond network (Tyr58, Tyr114, Arg136, and Asn210) and consequent displacement of water residues needed for catalysis.

Table 5
Docking results for molecules (*S*)-**1a–**k.

Compound	ΔG_B calcd. (kcal/mol)	K_i calcd. (μM)	Exp. IC_{50} (μM) HO-1
1a	–7.58	2.8	0.40
1b	–8.64	0.5	0.90
1c	–6.85	9.5	14.80
1d	–6.71	12.0	11.70
1e	–6.32	23.2	26.90
1f	–8.16	1.0	0.90
1g	–6.75	11.2	26.90
1h	–8.69	0.4	0.50
1i	–6.93	8.3	13.10
1j	–8.48	0.6	0.95
1k	–6.16	30.4	24.50

In the docked structures, the substituted phenylethanolic linker of our inhibitors is always located in the western region of the binding pocket, whereas the northeastern pocket remains free. The docking poses for the most potent and selective inhibitors **1a**,**b**,**j** are reported in Fig. 1.

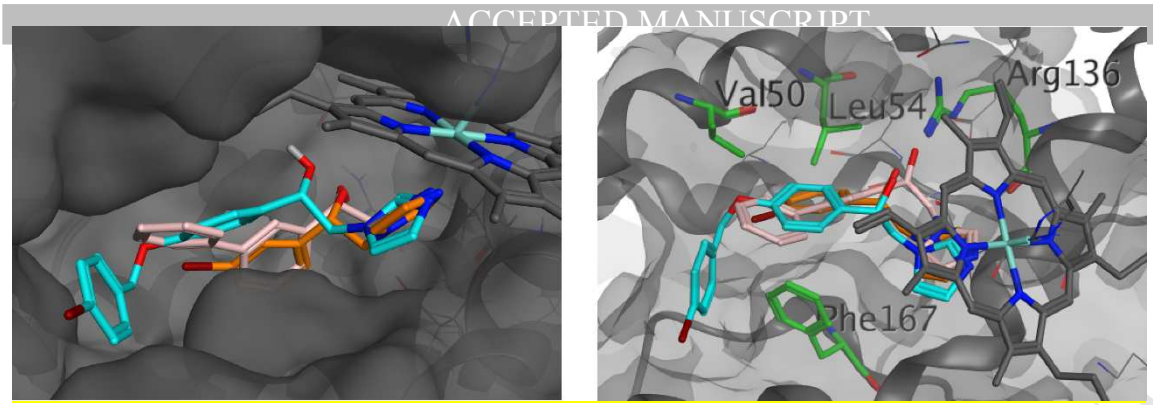

Fig. 1. Docked poses of compounds **1a** (orange), **1b** (pink), and **1j** (turquoise). Left: binding pocket full surface. Right: highlighted sidechains of the amino acids involved in the key interactions.

In particular, compound **1a** results as the most potent compound of the series, with a selectivity of 80 toward HO-2; the docking pose of **1a** revealed interactions similar to the classical HO-1 inhibitors, with the phenyl-connecting group in the principal western region pocket (Leu54, Phe167, Val50 and Arg 136) and the bromine pointing to the external portion inside the western region (Fig. S1). On the other hand, the second most selective compound **1j**, with a selectivity index HO-2/HO-1 >105, due to its length and volume, showed a slight difference in the calculated pose inside the protein with the former compound. In this case, the connecting phenyl group is in the western region of the binding site, but the secondary aromatic group (4-bromophenyl) is pointing to the external surface of the protein (Fig. S4). However, with the docking experiments it was verified that the secondary aromatic group is not located deep inside the western pocket, neither in this case and nor for compounds **1e** and **1g**–**k**. Also, the use of the co-crystallized form with QC-80, allow us to exclude even a pose with this secondary aromatic moiety inside the northeastern region. Finally, the most selective compound **1b** also shows a binding arrangement similar to the previous compounds. The aromatic linker portion is located at the bottom of the western cavity, while the phenyl in position 3 points to the outside of the cavity (Fig. S5).

2.5. ADME and toxicity risk assessment

To verify if the designed compounds showed a good pharmacokinetic profile and no adverse side effects (ADME-Toxicity), we conducted an *in silico* study for the compounds with the highest activity and selectivity **1a**,**b**,**j**. These results are reported in Tables 5 and 6 together with that of the best four compounds present in the HemOxDB.

The *in silico* ADME results (Table 5) clearly show that the new synthesized compounds should exhibit a good oral availability [human intestinal absorption (HIA) >70% and Caco-2 cell permeability >4) but with a strong plasma protein binding (PPB >90%), with the exception of **1a**, penalizing their diffusion and transport across cell membranes. Interestingly, compounds **1a**,**b**,**j** are supposed to discreetly permeate the blood-brain barrier (BBB penetration <1) making them, and especially **1a**, potential candidates for neuroblastoma therapy. Moreover, all these imidazole derivatives resulted non-mutagen, non-tumorigenic, non-irritant and without negative effects on the reproductive system (Table 6). Finally, all the three new synthesized compounds possess a positive value of drug-likeness, stating that the molecule predominantly contains fragments which are frequently present in commercial drugs, and a drug-score, that encompass the contributions of partition coefficient, solubility, molecular weight, drug-likeness and the four toxicity risk, higher than that of the four best compounds so far reported.

Table 5
Selected *in silico* ADME profiling of most selective compounds in HemOxDB and **1a**,**b**,**j**[a].

Compound	Absorption		Distribution	
	HIA (%)	*In vitro* Caco-2 cell permeability (nm s^{-1})	*In vitro* PPB (%)	*In vivo* BBB penetration (C_{brain}/C_{blood})
HemOxDB2	96.83	45.99	98.72	0.28
HemOxDB18	98.48	57.26	84.58	0.42
HemOxDB16	100.00	57.55	88.16	0.47
HemOxDB20	98.69	48.64	77.57	1.49
1a	96.07	29.63	65.33	0.72
1b	96.22	41.25	94.03	0.26
1j	96.58	47.67	90.94	0.10

[a] The properties related to ADME were predicted using PreADMET web-based application (http://preadmet.bmdrc.kr).

Table 6
I*n silico* toxicity parameters of most selective compounds in HemOxDB and **1a**,**b**,**j**[a].

	Mutagenic	Tumorigenic	Reproductive Effects	Irritant	Drug-Likeness	Drug-Score
HemOxDB2	none	none	none	none	3.05	0.77
HemOxDB18	none	none	high	low	4.07	0.42
HemOxDB16	none	none	none	none	0.63	0.72
HemOxDB20	none	none	none	none	–2.33	0.51
1a	none	none	none	none	3.05	0.92
1b	none	none	none	none	4.84	0.89

1j	none	none	none	none	2.65	0.79

[a] The properties related to toxicity were predicted using DataWarrior software [45].

3. Conclusion

In this study, we report the design, synthesis and biological properties of a series of imidazole-based derivatives **1a**–**k**. All of the obtained compounds were tested for their inhibitory activity in HO-1 and those which showed a HO-1 IC_{50} inhibitory activity <1 μM were tested on HO-2. Above all, compounds **1a**, **1b**, **1f**, **1h**, and **1j**, presented an IC_{50} <1 μM on HO-1 and **1b**,**j** showed a >100 selectivity toward HO-2, according to the design predictions. Modeling studies of these imidazole-based inhibitors proved that in all of the molecules the imidazole interacts with the iron of the heme group; moreover, all hydrophobic groups reside only in the principal western pocket and the most potent and selective compounds fill it almost completely. Moreover, *in silico* prediction of the ADME-Tox profiles for the most potent and selective compounds **1a**,**b**,**j** highlighted that they exhibit a good oral availability, a strong plasma protein binding, with the exception of **1a**, and a discrete capacity to permeate the BBB making them, and especially **1a**, potential candidates for neuroblastoma therapy. Moreover, all these imidazole derivatives resulted non-mutagen, non-tumorigenic, non-irritant and without negative effects on the reproductive system (Table 6). Finally, all the three new synthesized compounds possess an elevated value of drug-score, higher than that of the four best compounds so far reported, suggesting them as the new lead candidates for further studies.

4. Experimental section

4.1. Chemistry

Melting points were determined in an IA9200 Electrothermal apparatus equipped with a digital thermometer in glass capillary tubes and are uncorrected. Infrared spectra were recorded on a Perkin Elmer 281 FTIR spectrometer in KBr disks or NaCl crystal windows. Elemental analyses for C, H, N, and S were performed on a Carlo Erba Elemental Analyzer Mod. 1108 apparatus. Analyses

indicated by the symbols of the elements or functions were within ±0.4% of the theoretical values. ^{1}H NMR spectra were recorded on a Varian Unity Inova 200 or 500 MHz spectrometer in DMSO-d_6 solution. Chemical shifts are given in d values (ppm), using tetramethylsilane (TMS) as the internal standard; coupling constants (*J*) are given in Hz. Signal multiplicities are characterized as s (singlet), d (doublet), t (triplet), q (quartet), m (multiplet), br (broad). All the synthesized compounds were tested for purity on TLC (aluminum sheet coated with silica gel 60 F254, Merck) and visualized by UV (λ = 254 and 366 nm). Purification of synthesized compounds by column chromatography was performed using silica gel 60 (Merck). All chemicals and solvents were reagent grade and were purchased from commercial vendors.

*4.1.1. General procedure for the synthesis of 2-bromo-1-{4-[(4-bromobenzyl)oxy]phenyl}ethanone and 2-bromo-1-{4-[(4-iodobenzyl)oxy]phenyl}ethanone (**2j**,**k**)*

The appropriate commercially available 1-{4-[(4-bromobenzyl)oxy]phenyl}ethanone or 1-{4-[(4-iodobenzyl)oxy]phenyl}ethanone (5 mmol) was dissolved in 4 mL of glacial acetic acid, bromine (5 mmol) was added dropwise and the reaction mixture was stirred at 22 °C for 1 h. The obtained reaction mixture was dropped in saturated $NaHCO_3$, extracted with EtOAc (3 × 30 mL). The combined organic layers were dried over Na_2SO_4, filtered and evaporated. The obtained crude **2j**,**k** were used such as.

*4.1.2. General procedure for the synthesis of 1-substituted-2-(1H-imidazol-1-yl)ethanones (**3a**–**k**)*

The appropriate, 2-bromo-1-substituted ethanone (**2a**–**k**, 5 mmol), was dissolved in anhydrous DMF (15 mL) and added drop-wise to a previously prepared suspension of imidazole (15 mmol) and K_2CO_3 (15 mmol) in anhydrous DMF (30 mL). The obtained reaction mixture was left stirring for 2 h; then, water was added and the resulting suspension was filtered. The crude filtrate was purified by column chromatography using a Biotage® chromatographic system with Biotage® SNAP KP-Sil flash chromatography cartridges and DCM/methanol (98:2) as eluent. Analytical and spectral data are reported only for unknown compounds **3e** and **3i**–**k**. Compounds **3a**–**d**, and **3f**–**h** were previously reported in the literature [27, 40, 46].

*4.1.2.1. 1-(4'-chlorobiphenyl-4-yl)-2-(1H-imidazol-1-yl)ethanone (**3e**)*

The title compound was obtained as a pure white solid (49%): mp 189–191 °C; IR (KBr, selected lines) cm^{-1} 3102, 2921, 1696, 1686, 1602, 1487, 1392, 1235, 1097, 991, 813, 663; NMR (200 MHz, DMSO-d_6): 8.18–8.05 (m, 2H, aromatic), 7.95–7.78 (m, 4H, aromatic), 7.62–7.53 (m, 2H + 1H, aromatic + imidazole), 7.14 (s, 1H, imidazole), 6.94 (s, 1H, imidazole), 5.78 (s, 2H, CH_2). Anal. ($C_{17}H_{13}ClN_2O$) C, H, N.

*4.1.2.2. 1-{4-[(4-chlorobenzyl)oxy]phenyl}-2-(1H-imidazol-1-yl)ethanone (**3i**)*

The title compound was obtained as a pure white solid (52%): mp 118–119 °C; IR (KBr, selected lines) cm^{-1} 3130, 1690, 1600, 1508, 1235, 1176, 1086, 1015, 990, 810, 609; ^1H NMR (200 MHz, DMSO-d_6): 8.06–7.96 (m, 2H, aromatic), 7.58 (s, 1H, imidazole), 7.50–7.42 (s, 4H, aromatic), 7.20–7.15 (m, 2H, aromatic), 7.10 (s, 1H, imidazole), 6.91 (s, 1H, imidazole), 5.67 (s, 2H, CH_2N), 5.25 (s, 2H, CH_2O). Anal. ($C_{18}H_{15}ClN_2O$) C, H, N.

*4.1.2.3. 1-{4-[(4-bromobenzyl)oxy]phenyl}-2-(1H-imidazol-1-yl)ethanone (**3j**)*

The title compound was obtained as pure off-white solid (35%): mp 115–116 °C; IR (KBr, selected lines) cm^{-1} 3114, 1691, 1678, 1599, 1498, 1235, 1178, 1029, 992, 904, 807; ^1H NMR (200 MHz, DMSO-d_6): 8.07–7.95 (m, 2H, aromatic), 7.68–7.57 (s, 2H + 1H, aromatic + imidazole), 7.47–7.36 (m, 2H, aromatic), 7.20–7.15 (m, 2H, aromatic), 7.11 (s, 1H, imidazole), 6.92 (s, 1H, imidazole), 5.67 (s, 2H, CH_2N), 5.23 (s, 2H, CH_2O). Anal. ($C_{18}H_{15}BrN_2O$) C, H, N.

*4.1.2.4. 2-(1H-imidazol-1-yl)-1-{4-[(4-iodobenzyl)oxy]phenyl}ethanone (**3k**)*

The title compound was obtained as pure off-white solid (33%): mp 195–196 °C; IR (KBr, selected lines) cm^{-1} 3132, 3106, 1694, 1600, 1500, 1232, 1174, 1086, 1011, 989, 826,660; ^1H NMR (200 MHz, DMSO-d_6): 8.15–7.63 (m, 4H, aromatic), 7.61 (s, 1H, imidazole), 7.18–7.00 (m, 4H + 1H, aromatic + imidazole), 6.93 (s, 1H, imidazole), 5.68 (s, 2H, CH_2N), 5.22 (s, 2H, CH_2O). Anal. ($C_{18}H_{15}IN_2O$) C, H, N.

*4.1.3. General procedure for the synthesis of 1-(substituted)-2-(1H-imidazol-1-yl)ethanoles **1a–k***

A mixture of the appropriate imidazole-ketone (**3a**–**k**, 2.0 mmol) and $NaBH_4$ (2.2 mmol) in

anhydrous methanol (10 mL) was refluxed for 2 h; then it was evaporated to dryness, added with deionized water (40 mL), acidified with HCl 2N and heated to 110 °C for 0.5 h. After cooling to room temperature, the reaction mixture was treated with NaOH 0.5N up to a pH of 8–9 and the obtained suspension was filtered, washed repeatedly with water to neutrality, and dried. Using this procedure, the following compounds were obtained.

*4.1.3.1. 1-(3-bromophenyl)-2-(1H-imidazol-1-yl)ethanol (**1a**)*

Recrystallization from EtOH gave the title compound as a pure light yellow solid (72%): mp 109–111 °C; IR (KBr, selected lines) cm^{-1} 3122, 1567, 1508, 1418, 1233, 1105, 1065, 920, 750; ^{1}H NMR (500 MHz, DMSO-d_6): 7.54 (bs, 1H, imidazole), 7.50–7.48 (m, 1H, aromatic), 7.36–7.27 (m, 2H + 1H, aromatic), 7.11 (s, 1H, imidazole), 6.83 (s, 1H, imidazole), 5.83 (d, J = 5 Hz, 1H, OH), 4.88–4.80 (m, 1H, CH), 4.15 (dd, J = 14.5 Hz, J = 4 Hz, 1H, CH_ACH_B), 4.04 (dd, J = 8 Hz, J = 14 Hz, 1H, CH_ACH_B); ^{13}C NMR (125 MHz, DMSO-d_6) 145.42, 137.69, 130.25, 130.09, 128.79, 127.72, 125.035, 121.47, 120.00, 71.30, 53.18. Anal. ($C_{11}H_{11}BrN_2O$) C, H, N.

*4.1.3.2. 1-(biphenyl-3-yl)-2-(1H-imidazol-1-yl)ethanol (**1b**)*

Recrystallization from EtOH gave the title compound as a pure light brown sticky oil (90%): IR (KBr, selected lines) cm^{-1} 3117, 1512, 1484, 1390, 1233, 1080, 1003, 814, 747, 649; ^{1}H NMR (500 MHz, DMSO-d_6): 7.65–7.35 (m, 9H + 1H, aromatic + imidazole), 7.15 (s, 1H, imidazole), 6.85 (s, 1H, imidazole), 5.77 (bs 1H, OH), 4.93–4.88 (m, 1H, CH), 4.21 (dd, J = 14 Hz, J = 4 Hz, 1H, CH_ACH_B), 4.10 (dd, J = 8 Hz, J = 14 Hz, 1H, CH_ACH_B). ^{13}C NMR (125 MHz, DMSO-d_6) 143.29, 140.20, 139.94, 128.85, 128.65, 127.69, 127.39, 126.67, 125.63, 125.04, 124.45, 120.06, 72.05, 53.51. Anal. ($C_{17}H_{16}N_2O$) C, H, N.

*4.1.3.3. 2-(1H-imidazol-1-yl)-1-(4-iodophenyl)ethanol (**1c**)*

Recrystallization from EtOH gave the title compound as a pure off-white solid (88%): mp 182–183 °C; IR (KBr, selected lines) cm^{-1} 3116, 2933, 1512, 1484, 1399, 1280, 1231, 1073, 1102, 1073, 1006, 918, 818, 738; ^{1}H NMR (500 MHz, DMSO-d_6): 7.70–7.67 (m, 2H, aromatic), 7.46 (s, 1H, imidazole), 7.18–7.08 (m, 2H + 1H, aromatic + imidazole), 6.82 (s, 1H, imidazole), 5.78 (d, J = 4

Hz, 1H, OH), 4.82–4.78 (m, 1H, CH), 4.12 (dd, J = 14 Hz, J = 4 Hz, 1H, CH_ACH_B), 4.02 (dd, J = 8 Hz, J = 14 Hz, 1H, CH_ACH_B); ^{13}C NMR (125 MHz, DMSO-d_6) 142.38, 136.74, 128.37, 127.74, 120.00, 93.18, 71.43, 53.17. Anal. ($C_{11}H_{11}IN_2O$) C, H, N.

*4.1.3.4. 1-(biphenyl-4-yl)-2-(1H-imidazol-1-yl)ethanol (**1d**)*

Recrystallization from EtOH gave the title compound as a pure off-white solid (80%): mp 182–183 °C (183–184, lit. [46]); IR (KBr, selected lines) cm^{-1} 3188, 3110, 1511, 1488, 1282, 1234, 1075, 833, 753; ^{1}H NMR (500 MHz, DMSO-d_6): 7.69–7.61 (m, 4H, aromatic) 7.53 (s, 1H, imidazole), 7.49–7.41 (m, 5H, aromatic), 7.16 (s, 1H, imidazole), 6.85 (s, 1H, imidazole), 5.76 (d, J = 4.2 Hz, 1H, OH), 4.88–4.85 (m, 1H, CH), 4.19 (dd, J = 14 Hz, J = 4 Hz, 1H, CH_ACH_B), 4.08 (dd, J = 8 Hz, J = 14 Hz, 1H, CH_ACH_B), ^{13}C NMR (125 MHz, DMSO-d_6) 141.84, 139.85, 139.13, 137.72, 128.89, 127.74, 127.35, 126.63, 126.56, 126.33, 120.03, 71.82, 53.43. Anal. ($C_{17}H_{16}N_2O$) C, H, N.

*4.1.3.5. 1-(4'-chlorobiphenyl-4-yl)-2-(1H-imidazol-1-yl)ethanol (**1e**)*

Recrystallization from EtOH gave the title compound as a pure white solid (82%): mp 232–233 °C; IR (KBr, selected lines) cm^{-1} 3116, 1513, 1485, 1391, 1233, 1099, 1080, 1003,814, 649; ^{1}H NMR (500 MHz, DMSO-d_6): 7.76–7.63 (m, 4H, aromatic), 7.55–7.41(m, 4H + 1H, aromatic + imidazole), 7.16 (s, 1H, imidazole), 6.85 (s, 1H, imidazole), 5.76 (d, J = 4.5 Hz, 1H, OH), 4.18 (dd, J = 14 Hz, J = 4 Hz, 1H, CH_ACH_B), 4.07 (dd, J = 8 Hz, J = 14 Hz, 1H, CH_ACH_B); ^{13}C NMR (125 MHz, DMSO-d_6) 142.23, 138.63, 137.74, 132.21, 128.83, 128.30, 127.77, 126.69, 126.27, 71.74, 53.40. Anal. ($C_{17}H_{15}ClN_2O$) C, H, N.

*4.1.3.6. 2-(1H-imidazol-1-yl)-1-(4-phenoxyphenyl)ethanol (**1f**)*

Recrystallization from EtOH gave the title compound as a pure white solid (85%): mp 159–160 °C; IR (KBr, selected lines) cm^{-1} 3116, 1590, 1506, 1488, 1240, 1167, 1082, 1073, 834, 694; ^{1}H NMR (500 MHz, DMSO-d_6): 7.55–7.45 (m, 1H, imidazole), 7.40–7.30 (m, 4H, aromatic), 7.17–7.08 (m, 1H + 1H, aromatic + imidazole), 7.00–6.95 (m, 4H, aromatic), 6.83 (s, 1H, imidazole), 5.72 (d, J = 4.5 Hz, 1H, OH), 4.81 (m, 1H, CH), 4.13 (dd, J = 14 Hz, J = 4 Hz, 1H, CH_ACH_B), 4.04 (dd, J = 8 Hz, J = 14 Hz, 1H, CH_ACH_B). ^{13}C NMR (125 MHz, DMSO-d_6) 156.78, 155.73, 137.78, 129.98,

127.66, 123.30, 119.98, 118.38, 118.32, 71.56. Anal. ($C_{17}H_{16}N_2O_2$) C, H, N.

*4.1.3.7. 1-(4-benzylphenyl)-2-(1H-imidazol-1-yl)ethanol (**1g**)*

Recrystallization from EtOH gave the title compound as a pure off-white solid (90%): mp 159–160 °C; IR (KBr, selected lines) cm^{-1} 3118, 2921, 1510, 1494, 1417, 1235, 1079, 1017, 920, 733, 697; ^{1}H NMR (500 MHz, DMSO-d_6): 7.49 (s, 1H, imidazole), 7.35–7.02 (m, 9H, aromatic), 6.83 (s, 1H, imidazole), 6.84 (s, 1H, imidazole), 5.64 (bs, 1H, OH), 4.78–4.73 (m, 1H, CH), 4.10 (dd, J = 14 Hz, J = 4 Hz, 1H, CH_ACH_B), 4.00 (dd, J = 8 Hz, J = 14 Hz, 1H, CH_ACH_B), 3.92 (s, 2H, CH_2); ^{13}C NMR (125 MHz, DMSO-d_6) 141.29, 140.30, 128.60, 128.39, 128.36, 127.70, 126.12, 125.89, 71.91, 53.51. Anal. ($C_{18}H_{18}N_2O$) C, H, N.

*4.1.3.8. 1-[4-(benzyloxy)phenyl]-2-(1H-imidazol-1-yl)ethanol (**1h**)*

Recrystallization from EtOH gave the title compound as a pure white solid (92%): mp 145–146 °C; IR (KBr, selected lines) cm^{-1} 3115, 2886, 1612, 1509, 1454, 1255, 1238, 1171, 1076, 1045, 823, 731; ^{1}H NMR (500 MHz, DMSO-d_6): 7.50–7.29 (m, 5H + 1H, aromatic + imidazole), 7.26–7. –23 (m, 2H, aromatic), 7.09 (s, 1H, imidazole), 6.99–6.92 (m, 2H, aromatic), 6.82 (s, 1H, imidazole), 5.58 (bs, 1H, OH), 4.79–4.67 (m, 1H, CH), 4.09 (dd, J = 14 Hz, J = 4 Hz, 1H, CH_ACH_B), 4.01 (dd, J = 8 Hz, J = 14 Hz, 1H, CH_ACH_B); ^{13}C NMR (125 MHz, DMSO-d_6) 157.58, 137.10, 134.86, 128.37, 127.73, 127.60, 127.17, 114.34, 71.62, 69.12, 53.54. Anal. ($C_{18}H_{18}N_2O_2$) C, H, N.

*4.1.3.9. 1-{4-[(4-chlorobenzyl)oxy]phenyl}-2-(1H-imidazol-1-yl)ethanol (**1i**)*

The obtained crude material was purified by column chromatography using a Biotage® chromatographic system with Biotage® SNAP KP-Sil flash chromatography cartridges and DCM/methanol (98:2) as eluent, to afford the title compound as pure off-white solid (65%): mp 197–198 °C; IR (KBr, selected lines) cm^{-1} 3115, 1611, 1510, 1490, 1231, 1175, 1081, 1052, 1013, 822, 661; ^{1}H NMR (500 MHz, DMSO-d_6): 7.50–7.41 (m, 4H + 1H, aromatic + imidazole), 7.28–7.21 (m, 2H, aromatic), 7.09 (s, 1H, imidazole), 6.99–6.92 (m, 2H, aromatic), 6.82 (s, 1H, imidazole), 5.58 (d, J = 4 Hz, 1H, OH), 5.09 (s, 2H, CH_2), 4.78–4.71 (m, 1H, CH), 4.09 (dd, J = 14 Hz, J = 4 Hz, 1H, CH_ACH_B), 4.01 (dd, J = 8 Hz, J = 14 Hz, 1H, CH_ACH_B); ^{13}C NMR (125 MHz,

DMSO-d_6) 157.36, 137.63, 136.17, 135.01, 132.29, 129.39, 128.36, 127.66, 127.18, 119.95, 114.36, 71.60, 71.50, 68.27, 53.52. Anal. ($C_{18}H_{17}ClN_2O$) C, H, N.

*4.1.3.10. 1-{4-[(4-bromobenzyl)oxy]phenyl}-2-(1H-imidazol-1-yl)ethanol (**1j**)*

The obtained crude material was purified by column chromatography using a Biotage® chromatographic system with Biotage® SNAP KP-Sil flash chromatography cartridges and DCM/methanol (98:2) as eluant, to afford the title compound as a pure white solid (61%): mp 205–206 °C; IR (KBr, selected lines) cm^{-1} 3117, 1610, 1509, 1489, 1230, 1174, 1071, 1010, 821, 661; ^{1}H NMR (500 MHz, DMSO-d_6): 7.60–7.57 (m, 2H, aromatic), 7.46 (s, 1H, imidazole), 7.41–7.38 (m, 2H, aromatic), 7.28-7.20 (m, 2H, aromatic), 7.08 (s, 1H, imidazole), 6.98–6.92 (m, 2H, aromatic), 6.81 (s, 1H, imidazole), 5.58 (d, J = 4.5 Hz, 1H, OH), 5.07 (s, 2H, CH_2), 4.08 (dd, J = 14 Hz, J = 4 Hz, 1H, CH_ACH_B), 4.00 (dd, J = 8 Hz, J = 14 Hz, 1H, CH_ACH_B). ^{13}C NMR (125 MHz, DMSO-d_6) 157.34, 137.63, 135.02, 131.28, 129.69, 127.67, 127.18, 120.81, 119.94, 114.36, 71.60, 68.30, 53.51. Anal. ($C_{18}H_{17}BrN_2O$) C, H, N.

*4.1.3.11. 1-{4-[(4-iodobenzyl)oxy]phenyl}-2-(1H-imidazol-1-yl)ethanol (**1k**)*

The obtained crude material was purified by column chromatography using a Biotage® chromatographic system with Biotage® SNAP KP-Sil flash chromatography cartridges and DCM/methanol (98:2) as eluant, to afford the title compound as a pure white solid (89%): mp 197–198 °C; IR (KBr, selected lines) cm^{-1} 3116, 1610, 1508, 1458, 1231, 1077, 1008, 918, 802, 660; ^{1}H NMR (500 MHz, DMSO-d_6): 7.78–7.72 (m, 2H, aromatic), 7.47 (s, 1H, imidazole), 7.28–7.22 (m, 4H, aromatic), 7.08 (s, 1H, imidazole), 6.95–6.91 (m, 2H, aromatic), 6.82 (s, 1H, imidazole), 5.58 (d, J = 3.5 Hz, 1H, OH), 5.06 (s, 2H, CH_2), 4.78–4.70 (m, 1H, CH), 4.09 (dd, J = 14 Hz, J = 4 Hz, 1H, CH_ACH_B), 4.00 (dd, J = 8 Hz, J = 14 Hz, 1H, CH_ACH_B); ^{13}C NMR (125 MHz, DMSO-d_6) 157.35, 137.14, 136.97, 134.99, 128.76, 127.64, 127.18, 119.96, 114.37, 93.73, 71.60, 68.42, 53.53. Anal. ($C_{18}H_{17}IN_2O$) C, H, N.

4.2. Biology

4.2.1. Preparation of spleen and brain microsomal fractions

HO-1 and HO-2 were obtained, respectively, from rat spleen and brain as the microsomal fraction prepared by differential centrifugation; the dominance of HO-1 protein in the rat spleen and of HO-2 in the rat brain has been well documented [47-50]. These particular microsomal preparations were selected in order to use the most native (i.e., closest to *in vivo*) forms of HO-1 and HO-2. Spleen and brain (Sprague-Dawley rats) microsomal fractions were prepared according to the procedure outlined by Ryter et al. [51]. The experiments reported in the present paper complied with current Italian law and met the guidelines of the Institutional Animal Care and Use Committee of University of Catania (Italy). The experiments were performed in male Sprague-Dawley albino rats (150 g body weight and age 45 d). They had free access to water and were kept at room temperature with a natural photo-period (12 h light-12 h dark cycle). For measuring HO-1 and HO-2 activities, each rat was sacrificed and their spleen and brain were excised and weighed. A homogenate (15%, w/v) of spleens and brains pooled from four rats was prepared in ice-cold HO-homogenizing buffer (50 mM Tris buffer, pH 7.4, containing 0.25 M sucrose) using a Potter-Elvehjem homogenizing system with a Teflon pestle. The microsomal fraction of rat spleen and brain homogenate was obtained by centrifugation at 10,000g for 20 min at 4 °C, followed by centrifugation of the supernatant at 100,000g for 60 min at 4 °C. The 100,000g pellet (microsomes) was resuspended in 100 mM potassium phosphate buffer, pH 7.8, containing 2 mM $MgCl_2$ with a Potter-Elvehjem homogenizing system. The rat spleen and brain microsomal fractions were divided into equal aliquots, placed into microcentrifuge tubes, and stored at –80 °C for up to 2 months. Protein concentration of the microsomal fraction was determined by Lowry method [52].

4.2.2. Preparation of biliverdin reductase

Liver cytosol has been used as a source of biliverdin reductase (BVR). Rat liver was perfused through the hepatic portal vein with cold 0.9% NaCl, then it was cut and flushed with 2×20 mL of ice-cold PBS to remove all of the blood. Liver tissue was homogenized in 3 volumes of a solution containing 1.15% KCl w/v and Tris buffer 20 mM, pH 7.8 on ice. Homogenates were centrifuged at 10,000g, for 20 minutes at 4 °C. The supernatant was decanted and centrifuged at 100,000g for 1 h

at 4 °C to sediment the microsomes. The 100,000g supernatant was saved and then stored in small amounts at –80 °C after its protein concentration was measured.

4.2.3. Measurement of HO-1 and HO-2 enzymatic activities in microsomal fraction of rat spleen and brain

The HO-1 and HO-2 activities were determined by measuring the bilirubin formation using the difference in absorbance at 464 to 530 nm as described by Ryter et al. [51]. Reaction mixtures (500 μL) consisted of 20 mM Tris-HCl, pH 7.4, (1 mg/mL) microsomal extract, 0.5–2.0 mg/mL biliverdin reductase, 1 mM NADPH, 2 mM glucose 6-phosphate (G6P), 1 U G6P dehydrogenase, 25 μM hemin, 10 μL of DMSO (or the same volume of DMSO solution of test compounds to a final concentration of 100, 10, and 1 μM). Incubations were carried out for 60 min at 37 °C in a circulating water bath in the dark. Reactions were stopped by adding 1 volume of chloroform. After recovering the chloroform phase, the amount of bilirubin formed was measured with a double-beam spectrophotometer as OD464-530 nm (extinction coefficient, 40 mM/cm^{-1} for bilirubin). One unit of the enzyme was defined as the amount of enzyme catalyzing the formation of 1 nmol of bilirubin/mg protein/h.

4.3. Docking

4.3.1. Preparation of ligands

The 3D structures of ligands were built using Gabedit (2.4.8) software [53] and all geometries were fully optimized, in the same software, with the semi-empirical PM6 Hamiltonian [54] implemented in MOPAC2016 (17.130W) [55].

4.3.2. Docking protocol

Macromolecules and ligands, were prepared within YASARA; the point charges were initially assigned according to the AMBER14 force field [56], and then damped to mimic the less polar Gasteiger charges used to optimize the AutoDock scoring function. Fine docking was performed by applying the Lamarckian genetic algorithm (LGA) implemented in AutoDock. The ligand-centered maps were generated by the program AutoGrid with a spacing of 0.375 Å and dimensions that

encompass all atoms extending 5 Å from the surface of the ligand. All of the parameters were inserted at their default settings. In the docking tab, the macromolecule and ligand are selected, and GA parameters are set as ga_runs = 100, ga_pop_size = 150, ga_num_evals = 20000000, ga_num_generations = 27000, ga_elitism = 1, ga_mutation_rate = 0.02, ga_crossover_rate = 0.8, ga_crossover_mode = two points, ga_cauchy_alpha = 0.0, ga_cauchy_beta = 1.0, number of generations for picking worst individual = 10.

From the crystal structures of the HO-1/QC-xx complex, we retained only the chain B and the prosthetic-heme group. Because no water molecules are directly involved in complex stabilization they were not considered in the docking process. All protein amino acidic residues were kept rigid whereas all single bonds of ligands were treated as full flexible.

Appendix A. Supplementary data

Supplementary data related to this article can be found at https://doi.org/

References

[1] J.F. Ewing, M.D. Maines, Histochemical localization of heme oxygenase-2 protein and mRNA expression in rat brain, Brain Res. Protoc., 1 (1997) 165-174.

[2] G.M. Trakshel, R.K. Kutty, M.D. Maines, Purification and characterization of the major constitutive form of testicular heme oxygenase. The noninducible isoform, J. Biol. Chem., 261 (1986) 11131-11137.

[3] N.G. Abraham, A. Kappas, Pharmacological and clinical aspects of heme oxygenase, Pharmacol. Rev., 60 (2008) 79-127.

[4] A.M. Choi, J. Alam, Heme oxygenase-1: function, regulation, and implication of a novel stress-inducible protein in oxidant-induced lung injury, Am. J. Respir. Cell Mol. Biol., 15 (1996) 9-19.

[5] S.M. Keyse, L.A. Applegate, Y. Tromvoukis, R.M. Tyrrell, Oxidant stress leads to transcriptional activation of the human heme oxygenase gene in cultured skin fibroblasts, Mol. Cell. Biol., 10 (1990) 4967-4969.

[6] G.Q. Wang, H.L. Bonkovsky, A. de Lemos, F.J. Burczynski, Recent insights into the biological functions of liver fatty acid binding protein 1, J. Lipid Res., 56 (2015) 2238-2247.

[7] G. Floresta, V. Pistara, E. Amata, M. Dichiara, A. Marrazzo, O. Prezzavento, A. Rescifina, Adipocyte fatty acid binding protein 4 (FABP4) inhibitors. A comprehensive systematic review, Eur. J. Med. Chem., 138 (2017) 854-873.

[8] E. Amata, V. Pittalà, A. Marrazzo, C. Parenti, O. Prezzavento, E. Arena, S.M. Nabavi, L. Salerno, Role of the Nrf2/HO-1 axis in bronchopulmonary dysplasia and hyperoxic lung injuries, Clin. Sci. (Lond.), 131 (2017) 1701-1712.

[9] K.D. Croft, D. Zhang, R. Jiang, A. Ayer, S. Shengule, R.J. Payne, N.C. Ward, R. Stocker, Structural requirements of flavonoids to induce heme oxygenase-1 expression, Free Radic. Biol. Med., 113 (2017) 165-175.

[10] V. Pittalà, L. Vanella, L. Salerno, C. Di Giacomo, R. Acquaviva, M. Raffaele, G. Romeo, M.N. Modica, O. Prezzavento, V. Sorrenti, Novel Caffeic Acid Phenethyl Ester (Cape) Analogues as Inducers of Heme Oxygenase-1, Curr. Pharm. Des., 23 (2017) 2657-2664.

[11] V. Pittalà, L. Vanella, L. Salerno, G. Romeo, A. Marrazzo, C. Di Giacomo, V. Sorrenti, Effects of Polyphenolic Derivatives on Heme Oxygenase-System in Metabolic Dysfunctions, Curr. Med. Chem., (2017).

[12] V. Pistarà, G.M. Lombardo, A. Rescifina, A. Bacchi, F. D'Andrea, F. Punzo, Experimental and in silico characterization of a biologically active inososе, Struct. Chem., 24 (2013) 955-965.

[13] V. Pistarà, A. Rescifina, F. Punzo, G. Greco, V. Barbera, A. Corsaro, Design, Synthesis, Molecular Docking and Crystal Structure Prediction of New Azasugar Analogues of α-Glucosidase Inhibitors, Eur. J. Org. Chem., (2011) 7278-7287.

[14] V.K. Bhutani, R. Poland, L.D. Meloy, T. Hegyi, A.A. Fanaroff, M.J. Maisels, Clinical trial of tin mesoporphyrin to prevent neonatal hyperbilirubinemia, J. Perinatol., 36 (2016) 533-539.

[15] T. Morisawa, R.J. Wong, V.K. Bhutani, H.J. Vreman, D.K. Stevenson, Inhibition of heme oxygenase activity in newborn mice by azalanstat, Can. J. Physiol. Pharmacol., 86 (2008) 651-659.

[16] H.K. Na, Y.J. Surh, Oncogenic potential of Nrf2 and its principal target protein heme oxygenase-1, Free Radic. Biol. Med., 67 (2014) 353-365.

[17] D. Tibullo, I. Barbagallo, C. Giallongo, L. Vanella, C. Conticello, A. Romano, S. Saccone, J. Godos, F. Di Raimondo, G. Li Volti, Heme oxygenase-1 nuclear translocation regulates bortezomibinduced cytotoxicity and mediates genomic instability in myeloma cells, Oncotarget, 7 (2016) 28868-28880.

[18] L. Salerno, V. Pittalà, G. Romeo, M.N. Modica, M.A. Siracusa, C. Di Giacomo, R. Acquaviva, I. Barbagallo, D. Tibullo, V. Sorrenti, Evaluation of novel aryloxyalkyl derivatives of imidazole and 1,2,4-triazole as heme oxygenase-1 (HO-1) inhibitors and their antitumor properties, Bioorg. Med. Chem., 21 (2013) 5145-5153.

[19] L. Salerno, G. Romeo, M.N. Modica, E. Amata, V. Sorrenti, I. Barbagallo, V. Pittalà, Heme oxygenase-1: A new druggable target in the management of chronic and acute myeloid leukemia, Eur. J. Med. Chem., 142 (2017) 163-178.

[20] P. Nuhn, B.M. Kunzli, R. Hennig, T. Mitkus, T. Ramanauskas, R. Nobiling, S.C. Meuer, H. Friess, P.O. Berberat, Heme oxygenase-1 and its metabolites affect pancreatic tumor growth in vivo, Mol. Cancer, 8 (2009) 1-10.

[21] M. Dichiara, O. Prezzavento, A. Marrazzo, V. Pittalà, L. Salerno, A. Rescifina, E. Amata, Recent advances in drug discovery of phototherapeutic non-porphyrinic anticancer agents, Eur. J. Med. Chem., 142 (2017) 459-485.

[22] A.L. Furfaro, N. Traverso, C. Domenicotti, S. Piras, L. Moretta, U.M. Marinari, M.A. Pronzato, M. Nitti, The Nrf2/HO-1 Axis in Cancer Cell Growth and Chemoresistance, Oxid. Med. Cell. Longev., 2016 (2016) 1958174.

[23] L.J. Ignarro, B. Ballot, K.S. Wood, Regulation of soluble guanylate cyclase activity by porphyrins and metalloporphyrins, J. Biol. Chem., 259 (1984) 6201-6207.

[24] D. Luo, S.R. Vincent, Metalloporphyrins inhibit nitric oxide-dependent cGMP formation in vivo, Eur. J. Pharmacol., 267 (1994) 263-267.

[25] H.J.W. Vreman, R. J.; Stevenson, D. K, In Carbon Monoxide and Cardiovascular Function, CRC: Boca Raton, 2002; Chapter 15, p 273, (2002).

[26] M. Sugishima, Y. Higashimoto, T. Oishi, H. Takahashi, H. Sakamoto, M. Noguchi, K. Fukuyama, X-ray crystallographic and biochemical characterization of the inhibitory action of an imidazole-dioxolane compound on heme oxygenase, Biochemistry (Mosc.), 46 (2007) 1860-1867.

[27] M.N. Rahman, J.Z. Vlahakis, W.A. Szarek, K. Nakatsu, Z. Jia, X-ray crystal structure of human heme oxygenase-1 in complex with 1-(adamantan-1-yl)-2-(1H-imidazol-1-yl)ethanone: a common binding mode for imidazole-based heme oxygenase-1 inhibitors, J. Med. Chem., 51 (2008) 5943-5952.

[28] M.N. Rahman, J.Z. Vlahakis, D. Vukomanovic, W.A. Szarek, K. Nakatsu, Z.C. Jia, X-ray Crystal Structure of Human Heme Oxygenase-1 with (2R,4S)-2-[2-(4-Chlorophenyl)ethyl]-2-[(1H-imidazol-1-yl)methyl]-4[((5-trifluoromethylpyridin-2-yl)thio)methyl]-1,3-dioxolane: A Novel, Inducible Binding Mode, J. Med. Chem., 52 (2009) 4946-4950.

[29] G. Roman, M.N. Rahman, D. Vukomanovic, Z. Jia, K. Nakatsu, W.A. Szarek, Heme oxygenase inhibition by 2-oxy-substituted 1-azolyl-4-phenylbutanes: effect of variation of the azole moiety. X-ray crystal structure of human heme oxygenase-1 in complex with 4-phenyl-1-(1H-1,2,4-triazol-1-yl)-2-butanone, Chem. Biol. Drug Des., 75 (2010) 68-90.

[30] M.N. Rahman, J.Z. Vlahakis, D. Vukomanovic, W. Lee, W.A. Szarek, K. Nakatsu, Z. Jia, A novel, "double-clamp" binding mode for human heme oxygenase-1 inhibition, PLoS One, 7 (2012) e29514.

[31] M.N. Rahman, D. Vukomanovic, J.Z. Vlahakis, W.A. Szarek, K. Nakatsu, Z. Jia, Structural insights into human heme oxygenase-1 inhibition by potent and selective azole-based compounds, J. R. Soc. Interface, 10 (2013) 20120697.

[32] V. Pittalà, L. Salerno, G. Romeo, M.N. Modica, M.A. Siracusa, A focus on heme oxygenase-1 (HO-1) inhibitors, Curr. Med. Chem., 20 (2013) 3711-3732.

[33] E. Amata, A. Marrazzo, M. Dichiara, M.N. Modica, L. Salerno, O. Prezzavento, G. Nastasi, A. Rescifina, G. Romeo, V. Pittalà, Heme Oxygenase Database (HemeOxDB) and QSAR Analysis of Isoform 1 Inhibitors, ChemMedChem, 12 (2017) 1873-1881.

[34] V. Sorrenti, S. Guccione, C. Di Giacomo, M.N. Modica, V. Pittalà, R. Acquaviva, L. Basile, M. Pappalardo, L. Salerno, Evaluation of imidazole-based compounds as heme oxygenase-1 inhibitors, Chem. Biol. Drug Des., 80 (2012) 876-886.

[35] L. Salerno, V. Pittalà, G. Romeo, M.N. Modica, A. Marrazzo, M.A. Siracusa, V. Sorrenti, C. Di Giacomo, L. Vanella, N.N. Parayath, K. Greish, Novel imidazole derivatives as heme oxygenase-1 (HO-1) and heme oxygenase-2 (HO-2) inhibitors and their cytotoxic activity in human-derived cancer cell lines, Eur. J. Med. Chem., 96 (2015) 162-172.

[36] R.T. Kinobe, J.Z. Vlahakis, H.J. Vreman, D.K. Stevenson, J.F. Brien, W.A. Szarek, K. Nakatsu, Selectivity of imidazole-dioxolane compounds for in vitro inhibition of microsomal haem oxygenase isoforms, Br. J. Pharmacol., 147 (2006) 307-315.

[37] J.Z. Vlahakis, R.T. Kinobe, R.J. Bowers, J.F. Brien, K. Nakatsu, W.A. Szarek, Synthesis and evaluation of azalanstat analogues as heme oxygenase inhibitors, Bioorg. Med. Chem. Lett., 15 (2005) 1457-1461.

[38] J.Z. Vlahakis, R.T. Kinobe, R.J. Bowers, J.F. Brien, K. Nakatsu, W.A. Szarek, Imidazole-dioxolane compounds as isozyme-selective heme oxygenase inhibitors, J. Med. Chem., 49 (2006) 4437-4441.

[39] G. Roman, J.G. Riley, J.Z. Vlahakis, R.T. Kinobe, J.F. Brien, K. Nakatsu, W.A. Szarek, Heme oxygenase inhibition by 2-oxy-substituted 1-(1H-imidazol-1-yl)-4-phenylbutanes: effect of halogen substitution in the phenyl ring, Bioorg. Med. Chem., 15 (2007) 3225-3234.

[40] G. Roman, J.Z. Vlahakis, D. Vukomanovic, K. Nakatsu, W.A. Szarek, Heme oxygenase inhibition by 1-aryl-2-(1h-imidazol-1-yl/1h-1,2,4-triazol-1-yl)ethanones and their derivatives, ChemMedChem, 5 (2010) 1541-1555.

[41] V. Pittalà, M.A. Siracusa, M.N. Modica, L. Salerno, A. Pedretti, G. Vistoli, A. Cagnotto, T. Mennini, G. Romeo, Synthesis and molecular modeling of 1H-pyrrolopyrimidine-2,4-dione derivatives as ligands for the alpha1-adrenoceptors, Bioorg. Med. Chem., 19 (2011) 5260-5276.

[42] A. Carletta, A. Tilborg, L. Moineaux, J. de Ruyck, L. Basile, L. Salerno, G. Romeo, J. Wouters, S. Guccione, How does binding of imidazole-based inhibitors to heme oxygenase-1 influence their conformation? Insights combining crystal structures and molecular modelling, Acta Crystallographica Section B-Structural Science Crystal Engineering and Materials, 71 (2015) 447-454.

[43] G.M. Morris, R. Huey, W. Lindstrom, M.F. Sanner, R.K. Belew, D.S. Goodsell, A.J. Olson, AutoDock4 and AutoDockTools4: Automated Docking with Selective Receptor Flexibility, J. Comput. Chem., 30 (2009) 2785-2791.

[44] E. Krieger, G. Vriend, YASARA View-molecular graphics for all devices-from smartphones to workstations, Bioinformatics, 30 (2014) 2981-2982.

[45] T. Sander, J. Freyss, M. von Korff, C. Rufener, DataWarrior: an open-source program for chemistry aware data visualization and analysis, J. Chem. Inf. Model., 55 (2015) 460-473.

[46] D. Nardi, A. Tajana, A. Leonardi, R. Pennini, F. Portioli, M.J. Magistretti, A. Subissi, Synthesis and anticonvulsant activity of N-(benzoylalkyl)imidazoles and N-(omega-phenyl-omega-hydroxyalkyl)imidazoles, J. Med. Chem., 24 (1981) 727-731.

[47] M.D. Maines, Heme oxygenase: function, multiplicity, regulatory mechanisms, and clinical applications, FASEB J., 2 (1988) 2557-2568.

[48] G.M. Trakshel, R.K. Kutty, M.D. Maines, Resolution of the rat brain heme oxygenase activity: absence of a detectable amount of the inducible form (HO-1), Arch. Biochem. Biophys., 260 (1988) 732-739.

[49] J.Z. Vlahakis, C. Lazar, G. Roman, D. Vukomanovic, K. Nakatsu, W.A. Szarek, Heme oxygenase inhibition by alpha-(1H-imidazol-1-yl)-omega-phenylalkanes: effect of introduction of heteroatoms in the alkyl linker, ChemMedChem, 7 (2012) 897-902.

[50] Z.W. Xia, W.J. Cui, X.H. Zhang, Q.X. Shen, J. Wang, Y.Z. Li, S.N. Chen, S.C. Yu, Analysis of heme oxygenase isomers in rat, World J. Gastroenterol., 8 (2002) 1123-1128.

[51] S.W. Ryter, J. Alam, A.M. Choi, Heme oxygenase-1/carbon monoxide: from basic science to therapeutic applications, Physiol. Rev., 86 (2006) 583-650.

[52] O.H. Lowry, N.J. Rosebrough, A.L. Farr, R.J. Randall, Protein measurement with the Folin phenol reagent, J. Biol. Chem., 193 (1951) 265-275.

[53] A.R. Allouche, Gabedit-A Graphical User Interface for Computational Chemistry Softwares, J. Comput. Chem., 32 (2011) 174-182.

[54] J.J.P. Stewart, Optimization of parameters for semiempirical methods V: Modification of NDDO approximations and application to 70 elements, J. Mol. Mod., 13 (2007) 1173-1213.

[55] J.J.P. Stewart, MOPAC2016, in, Stewart Computational Chemistry, Colorado Springs, CO, USA, 2016.

[56] Y. Duan, C. Wu, S. Chowdhury, M.C. Lee, G. Xiong, W. Zhang, R. Yang, P. Cieplak, R. Luo, T. Lee, J. Caldwell, J. Wang, P. Kollman, A point-charge force field for molecular mechanics simulations of proteins based on condensed-phase quantum mechanical calculations, J. Comput. Chem., 24 (2003) 1999-2012.